Magnetic interaction in pairwise Mn-doped Si nanocrystals

C. Panse,* R. Leitsmann,† and F. Bechstedt
European Theoretical Spectroscopy Facility (ETSF) and Institut für Festkörpertheorie und -optik, Friedrich-Schiller-Universität Jena, Max-Wien-Platz 1, 07743 Jena, Germany

(Received 31 May 2010; revised manuscript received 6 August 2010; published 10 September 2010)

The electronic-structure and magnetic properties of hydrogenated silicon nanocrystals doped with pairs of manganese atoms are investigated using spin-density-functional theory. Formation energies and total magnetic moments sensitively depend on the two sites occupied by manganese. Usually pairs at interstitial and substitutional sites with small total moment are energetically favored. Pairs at sites with the same character tend to ferromagnetic spin arrangements which are, however, significantly influenced by their noncollinearity. The resulting magnetic ordering is clearly related to the impurity levels and their occupation. The magnetic coupling is distance dependent, antiferromagnetic for small distances, and almost ferromagnetic for larger Mn-Mn distances. A Rudderman-Kittel-Kasuya-Yoshida-type exchange mechanism may describe the distance dependence but simultaneously not its magnitude.

DOI: 10.1103/PhysRevB.82.125205 PACS number(s): 75.50.Pp, 61.72.−y, 73.22.−f, 75.30.Hx

I. INTRODUCTION

Doping with impurities is a fundamental approach to modify the electronic properties of bulk semiconductors especially silicon. With the interest in spintronics doping of bulk silicon (Si) with transition-metal (TM) atoms attracted more and more attention. Especially, one tried to achieve above room-temperature ferromagnetism by incorporation of Manganese (Mn) into silicon crystals.[1] There were also predictions[2] that Si heterostructures with Mn δ doping should give rise to a two-dimensional ferromagnetic half metal. In general the reduction in the dimension into nanometer scale may lead to significant changes in the fundamental materials properties.[3] This also holds for semiconductor nanostructures. Important examples are TM-doped nanocrystals (NCs) with three-dimensional electronic confinement.[3–6] Their novel magnetic properties make them attractive to develop nanoscale magnetic species for spintronics.[7] Prototypical examples are prepared by incorporation of Mn^{2+} ions with the largest magnetic moment of the 3*d* shell into II-VI semiconductor nanocrystals.[3–6] Such doped nanocrystalline systems have also been studied theoretically.[7–9] Meanwhile such studies also exist for Mn-doped III-V semiconductor nanocrystals[8,10–12] and the incorporation of TM atoms into group-IV (Si or Ge) nanocrystals.[8,13–15] They are driven by experimental findings that, e.g., self- organized $Ge_{1-x}Mn_x$ nanocolumns show high-Curie-temperature ferromagnetism.[16]

The understanding of the magnetic and electronic properties of TM-doped nanostructures is related to the central question of interplay of electron confinement and magnetism on a nanoscale. Silicon NCs doped with Mn atoms represent appropriate model systems. Undoped and doped Si nanocrystals, which were constructed by taking spherical or facetted fragments of bulk material and passivated using hydrogen, have been applied for years to model electronic, optical, and electric properties of nanostructures. Doping with Mn impurities may give rise to large local magnetic moments according to Hund's rule, at least if the five Mn 3*d* electrons do not essentially contribute to the chemical bonding. The relationship of the electronic and magnetic properties to the different inequivalent sites has been studied for individual Mn dopants and differently sized NCs in detail.[13–15] Open questions concern the favored geometrical arrangement of TM atoms for higher dopant concentrations and the accompanying magnetic interactions as well as their modification with the NC size.

In bulk and layered Si-Mn systems a strong interaction of the TM 3*d* atomic shells with the surrounding sp^3 states, i.e., an almost *p-d* exchange interaction, has been found.[17–19] However, for Mn-doped nanocrystalline Ge a magnetic interaction different from that of the bulk has been predicted.[8] Instead of a Zener-type picture of interaction mediation by free holes[20] or a Rudderman-Kittel-Kasuya-Yoshida (RKKY) picture of interaction with free carriers[21] a double-exchange mechanism via localized holes seems to be more favorable.[8] In addition, the magnetic interaction of two Mn atoms and, hence, the lowest-energy configuration of their local moments, parallel or antiparallel (or more complex), may depend on the impurity distance and the site character, interstitial or substitutional.

In this paper the magnetic interactions on the nanoscale are studied for model systems of hydrogen-passivated Si NCs doped with pairs of Mn atoms. They are investigated in the framework of spin-polarized density-functional theory (DFT) and the generalized gradient approximation (GGA) for a semilocal description of exchange and correlation (XC). Effects of the noncollinearity of spins are taken into account. Additional strong electron-correlation effects are studied via a Hubbard-type Coulomb repulsion *U* since their influence on the total spin moments is strong for sufficiently small geometrical distortions.[14] Correspondingly, there is a remarkable influence on the (especially the Mn 3*d*-derived) impurity states but not on the NC states with almost Si-derived character. The interaction mechanisms are discussed versus the site character, the Mn-Mn distance, and the resulting electronic-level schemes.

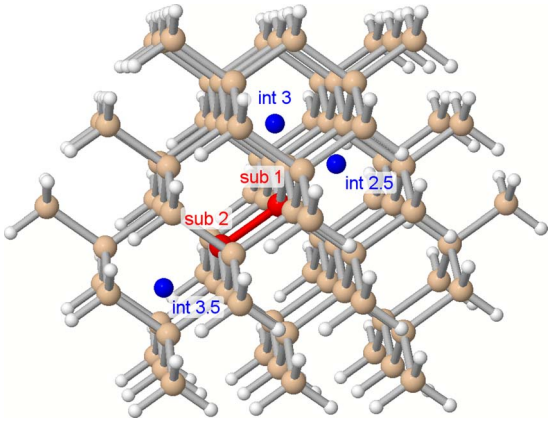

FIG. 1. (Color online) Schematic representation of the five-shell Si NC. The positions of the selected dopant sites are indicated by red (substitutional) and blue (interstitial) dots.

II. METHODS

A. Modeling

A free-standing nanocrystal is modeled via the supercell approach[22] in a simple-cubic arrangement. An edge lengths of 2.4 nm leads to a distance larger than 1.2 nm between the surfaces of the NCs. In order to study magnetic-coupling effects we restrict the studies to pairwise doped NCs. The geometry is built shell by shell, i.e., by starting from the central atom, adding Si atoms in a local tetrahedron coordination, and subsequent structural optimization. The passivation of the surface dangling bonds is done by hydrogen atoms. This procedure leads to NCs with varying total number of shells. Their shape is dominated by six rectangular {100} facets and eight triangular {111} facets. To allow a sufficient number of Mn combinations while keeping the numerical effort low, the largest nano-object for which we present results is the five-shell NC ($Si_{83}H_{108}$) with a nominal diameter of 2 nm, (including the hydrogen passivation shell). For two Mn dopants the doping concentration amounts approximately to 2.4%. A detailed description of the construction of pure Si NCs can be found elsewhere.[23,24]

Some of the possible dopant positions are marked in Fig. 1 either with red (substitutional) or blue (interstitial) atoms. To distinguish different individual dopant positions we use the notation (*type n*). The *type* can be either "sub" or "int" for a substitutional and an interstitial position, respectively. The radial position is given by the shell number $n \leq 5$, where $n=1$ indicates the position in the NC center. This number could be an integer, e.g., all substitutionals or interstitials beneath rectangular facets, or a half integer, if the dopant occupies a site between two Si shells, e.g., interstitials beneath triangular facets. The notation for the different Mn-Mn combinations is derived from the isolated Mn-atom case: *type A-B*: *g*. The type could be "sub," "mix," or "int," representing the three possible combinations of substitutional and interstitials. The shell numbers of both dopants are given by A and B. To distinguish between different inequal A-B combinations we introduce the geometrical degeneracy "*g*," which counts the possibilities to place the dopant B relative to A so that the resulting (type A-B) NCs are identical.

B. Computational aspects

The total-energy calculations of the doped silicon nanocrystals were done by first-principles techniques using the noncollinear formulation of the spin-polarized DFT as it is implemented in the Vienna *ab initio* simulation package (VASP).[25,26] Noncollinearity of the spin polarization is taken into account right from the beginning, i.e., the full vector of the local magnetization density and not only its *z* component is studied. There are indications that such effects are important for Mn-containing materials. Not only former studies on bulk Mn has shown that α-Mn metal possesses a noncollinear magnetic ground state but calculations on Mn clusters[27,28] and the Mn_5Ge_3 compound[29,30] also benefit from a noncollinear treatment in order to explain experimentally observed magnetic moments.

The pseudopotentials are generated by means of the projector-augmented-wave method[31] that allows for the accurate treatment of the Mn 3*d*, Mn 4*s*, Si 3*s*, and Si 3*p* valence electrons. In the region between the atomic cores the wave functions are expanded in plane waves up to a cutoff energy of about 300 eV.

To approximate the XC functional we use the generalized gradient approximation including an additional Coulomb repulsion *U* (GGA+*U*) (Ref. 32) for the electronic-structure calculations and the optimization of the atomic geometries. Especially the description of the strongly localized *d* electrons benefits from this treatment.[15] The Hubbard-type Coulomb repulsion *U* on the Mn 3*d* shell is set to a value of 3 eV. A detailed discussion on the influence of *U* for single TM-doped Si systems and how it compare to hybrid functionals (HSE03) could be found elsewhere.[15,19] This *U* value is proposed to be appropriate in the case of Mn-doped GaAs (Ref. 11) and sustained by photoemission experiments.[33] For intermediate spin polarizations we apply the interpolation proposed by von Barth and Hedin.[34] Since the used supercells are large, the **k**-point mesh in the reciprocal space can be restricted to the center of the Brillouin zone (Γ point). The structures of the NCs are optimized by means of the conjugate gradient algorithms. The atomic forces are minimized up to 20 meV/Å or less. The approach has been tested for Mn doping of bulk Si.[19] Good agreement with other recent first-principles calculations[19,35,36] was found, at least with respect to the atomic geometries and magnetic moments.

As the calculations include noncollinearity the magnetic density is treated as a three-dimensional vector field. The projected magnetic moments $\mathbf{m}_1$ and $\mathbf{m}_2$ are calculated as the integral around the special dopant site (integration radius 3.5 Å). The total magnetic moment (absolute value) is expressed by m_{tot} as integral over the whole supercell.

III. RESULTS

A. Formation energy

To compare the different types of Mn dimers embedded in Si NCs with respect to their relative stability and different preparation conditions we introduce the relative formation energy γ_f of the system. In general, one has to evaluate the total formation energy Ω_f for a doped Si NC containing

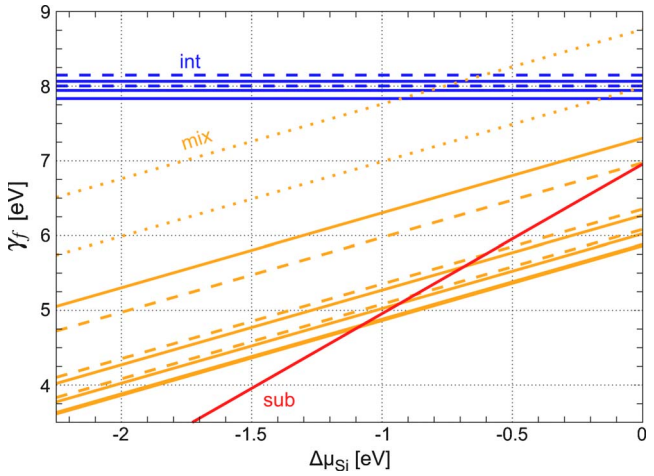

FIG. 2. (Color online) Formation energy of embedded Mn_2 dimers grouped according to the type of the dopant site: int, mix, and sub. Noncollinear magnetic ground states are indicated by dashed lines and asymmetric magnetizations ($m_1 \neq m_2$) by dotted lines. Detailed assignment could be done via the axial sections γ_f^0 given in Table I.

$N_{Si:Mn}$ silicon atoms and N_{Mn} manganese atoms. The possible preparation conditions are described by the chemical potentials μ_{Si} and μ_{Mn} of the corresponding reservoirs. It holds

$$\Omega_f = \gamma_f - N_{Mn}\mu_{Mn} \tag{1}$$

with

$$\gamma_f = E_{tot}^{Si:Mn} - E_{tot}^{Si} + (N_{Si} - N_{Si:Mn})\mu_{Si}, \tag{2}$$

where E_{tot}^X and N_X are the total energy and the number of silicon atoms in the doped (X=Si:Mn) and undoped (X=Si) Si NCs. The use of only the relative formation energy Eq. (2) is sufficient for discussion because the number of manganese atoms is constant (N_{Mn}=2) throughout the various calculations. By choosing the silicon bulk chemical potential μ_{Si}^{bulk} as an appropriate reference point we can discuss the relative formation energy with respect to the relative chemical potential $\Delta\mu_{Si}=\mu_{Si}-\mu_{Si}^{bulk}$ ($\Delta\mu_{Si}\leq 0$). For extremely Si-rich preparation conditions it holds $\mu_{Si}=\mu_{Si}^{bulk}$ with the relative chemical potential γ_f^0, which converts Eq. (2) to

$$\gamma_f = \gamma_f^0 + (N_{Si} - N_{Si:Mn})\Delta\mu_{Si} = \begin{cases} \gamma_f^0, & \text{int} \\ \gamma_f^0 + \Delta\mu_{Si}, & \text{mix} \\ \gamma_f^0 + 2\Delta\mu_{Si}, & \text{sub} \end{cases} \tag{3}$$

for the three different possibilities to arrange the Mn atoms on interstitial and substitutional sites. The formation energies resulting for the studied Mn-Mn combinations are presented in Fig. 2 and Table I. Comparing int-, mix-, and sub-type Mn dimers we found that the int-type ones are energetically unfavored at the whole scale of $\Delta\mu_{Si}$, i.e., Si-preparation conditions. Thereby, due to the relative large Mn-Mn distance ($d>3.75$ Å) the energy variation with distance is smaller than ΔE_{int}=300 meV. As a consequence of the restriction to inner interstitials inside a relatively large nanocrystal (without allowing a surface position) the weak energy variation

TABLE I. Formation energy γ_f^0 in the Si-rich preparation limit ($\Delta\mu_{Si}$=0) and Mn-Mn distance d grouped by the dimer type (int, mix, and sub)

	γ_f^0 (eV)	d (Å)
int 3.5–3.5:3	8.148	7.68
int 2.5–3.5:3	8.065	4.39
int 2.5–3.5:1	8.003	7.13
int 2.5–2.5:3	7.943	3.62
int 3–3:4	7.834	3.75
mix 1–3:6	8.760	2.94
mix 2–3:3	7.989	2.38
mix 1–3.5:4	7.303	4.76
mix 2–2.5:1	6.974	4.98
mix 2–2.5:3	6.353	2.80
mix 3–2.5:1	6.271	2.41
mix 2–3.5:1	6.083	2.53
mix 4–3:1	6.024	2.70
mix 1–2.5:4	5.882	2.52
mix 3–3:2	5.863	2.87
sub 1–2:4	6.956	2.92

reflects the beginning transition to the isolated bulk limit, where all interstitials are equal. Additionally the weak magnetic coupling for distances larger than 3.5 Å is keeping ΔE_{int} low. The high-energy value of int-type systems making those systems unfavorable is in good agreement with former results of Bernardini *et al.*[37]

Due to the stronger electronic and magnetic coupling of the mix-type dimers their formation energies in Fig. 2 and Table I are clearly spread over a bigger energy interval than the int-type ones. Restricting on symmetrical magnetizations we find a mix-type energy range of about ΔE_{mix}=1.4 eV. It turns out that the antiferromagnetic (AFM) mix 1–2.5 {111} and mix 3–3 {100} configurations with noncollinear deviations of the orientation of the local magnetizations smaller than 4° are the most favorable ones. Indeed, the total magnetic moment of the doped NC is almost vanishing with 0.3 μ_B and 0.0 μ_B, respectively. Although the two mixed Mn pairs exhibit rather identical formation energies their Mn-Mn distances are different with d=2.52 and 2.87 Å. So the mostly free adjustable Mn-Mn distance in mix-type dimers do not dominate the stabilization of such a system. The dominant effects are the local environment and the relative orientation of the embedded dimer.

The most stable Mn pair at not too far substitutional sites, sub 1–2:4, gives rise to rather low formation energies. In complete contrast to the isolated Mn impurities in bulk Si,[19] pairs of interstitial Mn dopants cannot become energetically favorable for Si-rich preparation conditions. In Fig. 2 one observes a transition from antiferromagnetic mix dimers toward the ferromagnetic (FM) sub 1–2 dimer if the relative chemical potential of silicon falls below $\Delta\mu_{Si}$=−1.1 eV. In order to illustrate this behavior we compare this transition

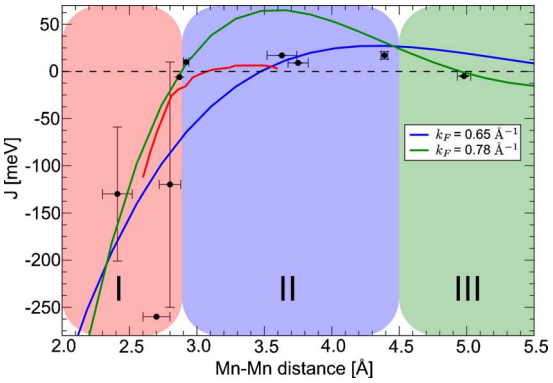

FIG. 3. (Color online) Magnetic coupling constant J as a function of the Mn-Mn distance d. Indicated are the three regions which exhibit (I) antiferromagnetic, (II) ferromagnetic, and (III) noncollinear magnetism. Only combinations with at least two converged magnetic orderings with approximately symmetric magnetizations ($|\mathbf{m}_1| \approx |\mathbf{m}_2|$) are considered. The dots are the values derived by means of Eq. (4) from the *ab initio* energies. The error bars are explained in the text. The results of Mejía-López *et al.* (Ref. 38) for free-standing Mn dimers are drawn as intermediate red line. Two curves which fit to the RKKY model [Eq. (5)] are drawn as blue and green lines. Their corresponding k_F values are given in the inset.

value $\Delta\mu_{\mathrm{Si}}$ to the result for the single-doped case. Since the mix-to-sub transition could be seen as the transition of a mix 1–2.5 toward a sub 1–2 we expect $\Delta\mu_{\mathrm{Si}}$ at the same value as for the mix 2.5—sub 2 (single-doped) transition, if the interaction of the Mn atoms is negligible. Actually the formation energies of isolated substitutional and interstitial Mn crosses at $\Delta\mu_{\mathrm{Si}}=-0.4$ eV.[14] The difference between the two values $\Delta\mu_{\mathrm{Si}}$ of 0.7 eV may be traced back to the magnetic coupling between two Mn atoms.

B. Magnetic coupling

To investigate magnetic exchange interactions we use the Heisenberg Hamiltonian

$$H = -\sum_{ij} J_{ij}\mathbf{S}_i \cdot \mathbf{S}_j \tag{4}$$

with effective Mn spins $\mathbf{S}_i$ with $\mathbf{m}_i = g\mu_{\mathrm{B}}\mathbf{S}_i$ and $g \approx 2$, which simplifies of only two magnetic atoms to $J_{ii}=0$ and $J=J_{12}=J_{21}$. The ground-state energies of different magnetic configurations (see Table I) can then be used to estimate the magnetic coupling constant J for a given configuration. In this work we focus on the dependence of this coupling constant on the Mn-Mn distance. The results are summarized in Fig. 3 and Table II. The occurrence of more than two converged magnetic configurations is indicated by an energetic uncertainty of J in Fig. 3. The fact that different magnetic orderings would affect the Mn-Mn distance is also reflected by an additional "error bar." This magnetically induced lattice deformation can change the Mn-Mn distance up to 8%.

The main feature of Fig. 3 is the crossing between the antiferromagnetic and ferromagnetic regions at the characteristic distance $d_c=2.9$ Å. As a result of the enhanced wavefunction overlap Mn_2 dimers with a distance $d<d_c$ (region I) exhibit an antiferromagnetic behavior of the local magnetic moments. The magnetic coupling constant J covers a wide range of negative values up to −260 meV. Thereby the numerical uncertainty is quite large reflecting the difficult convergence of the magnetization density for small distance dimers. The characteristic distance d_c remains slightly above the nearest-neighbor distance of 2.26 Å in bulk Mn and the distance 2.35–2.47 Å of Si nearest neighbors in the NC. For free-standing Mn_2 dimers the characteristic distance is about 3.06 Å.[38] Below this distance Mejía-López *et al.*[38] found an oscillating behavior of the total energy of the magnetic dimer but a clear favorization of the antiferromagnetic arrangement of the Mn spins. The complex interplay of the different contributing energy terms (exchange, correlation, kinetic energy, Coulomb energy, and core-core repulsion) leads to a sensitive distance dependence of the total energy, thereby generating strong fluctuations of the magnetic coupling constant J. Due to the coupling of substitutional Mn dopants with the

TABLE II. The magnetic properties, i.e., total magnetic moment m_{tot} of the doped NC, projections on the both Mn atoms m_1 and m_2, and the orientation angle $\alpha = \sphericalangle(\mathbf{m}_1, \mathbf{m}_2)$ of the two local magnetic moments are listed with respect to the Mn-Mn distance d. Additionally the number of shared energy levels N_{SEL} is indicated. As in Fig. 3 the three regions of different magnetic ordering are separated.

	d (Å)	m_{tot} (μ_{B})	m_1 (μ_{B})	m_2 (μ_{B})	α (deg)	J (meV)	N_{SEL}
mix 3–2.5:1	2.41	0.0	4.1	4.0	180	−130	3
mix 4–3:1	2.70	0.0	4.4	4.1	180	−260	2
mix 3–3:2	2.87	0.0	4.4	4.1	180	−6	1
sub 1–2:4	2.92	8.0	4.2	4.2	1	10	18
int 2.5–2.5:3	3.62	6.0	3.3	3.3	1	17	40
int 3–3:4	3.75	6.0	3.2	3.2	0	9	42
int 2.5–3.5:3	4.39	6.0	3.2	3.2	2	17	15
mix 2–2.5:1	4.98	1.0	4.2	4.0	168	−5	1
int 2.5–3.5:1	7.13	0.8	3.1	3.0	165		6
int 3.5–3.5:3	7.68	1.8	3.0	3.0	144		8

surrounding Si atoms via their *d-p* hybridization, the sensitive interplay of various energy contributions is further amplified for embedded Mn dimers. Surprisingly the presence of a Si matrix only weakly influences the transition distance d_c itself.

With rising distance (region II) the favored magnetic ordering becomes ferromagnetic with $J>0$ while the absolute values of the coupling constant decrease by about one order of magnitude to a maximum value $J=+17$ meV. Up to $d=4.5$ Å the effective magnetic coupling remains strong enough to buildup a global spin-quantization axis, i.e., the magnetic ordering remains almost collinear. In this distance range the sensitive energy behavior mentioned above vanishes for both the free and embedded Mn_2 dimers, thereby decreasing the uncertainty of J. Similar values are also observed for other Mn-containing systems. As shown by Strandberg *et al.*[11] for Mn doping of bulk GaAs the absolute value of J depends significantly on the Mn concentration and the chosen Hubbard U parameter. They report a increase in J from 19 to 55 meV if the concentration drops from 8% to 0.1%, i.e., varying the average distance of two Mn atoms between 2.8 and 12.2 Å. The lower value in our calculations reflects the weaker magnetic coupling in a silicon environment compared to the polar GaAs.

As the distance becomes larger (region III) the *d-d* coupling (between the Mn pair) becomes vanishing. In the first two distance regions (see Fig. 3) the *d*-level-driven exchange creates the observed collinear behavior. The electronic interaction of the Mn atoms toward the nearest-neighbor Si atoms (*p-d* coupling) starts to prevail for distances above 4.5 Å. As a consequence, the influence of the surrounding crystal (the local geometry) becomes more important. The magnetic moments lining up along (separate) high-symmetry directions of the NC, therefore building up noncollinear spin alignments with an angle deviation relative to the collinear case larger than 10°, as for the int 3.5–3.5 combination shown in Fig. 4. However the magnetic exchange remains strong enough to perform an additional sign change as expected for a RKKY-type behavior, e.g., the mix 2–2.5 configuration exhibits a slightly negative coupling constant J with a low uncertainty. Although the spin alignment could not be called AFM anymore (due to the noncollinear arrangement) the alignment character remains antiparallel with angles down to 144° (Fig. 4). For the two large distance int-type combinations (third group in Table II) a calculation of J is not possible anymore, because the involvement of dopant sites near the surface and the weak Mn-Mn coupling mentioned above. The energy term described in Eq. (4) is then prevailed by near-surface distortions.

A similar behavior as the transition from the region II into the region III has been observed experimentally for cobalt dimers on a copper surface with interatomic distances of 2.6–8.1 Å.[39] The overall results for J as a function of the distance are in good agreement with the magnetic coupling in the free-standing Mn_2 dimers calculated by Mejía-López *et al.*,[38] as shown in Fig. 3. The qualitative agreement shows that for Mn-Mn distances up to 4.5 Å the environmental influence is weak, except the slightly larger extent of region I. So embedding a Mn_2 dimer will hardly affect the magnetic interactions until the *p-d* (Mn-Si) hybridization prevails the *d-d* (Mn-Mn) coupling for distances above 4.5 Å.

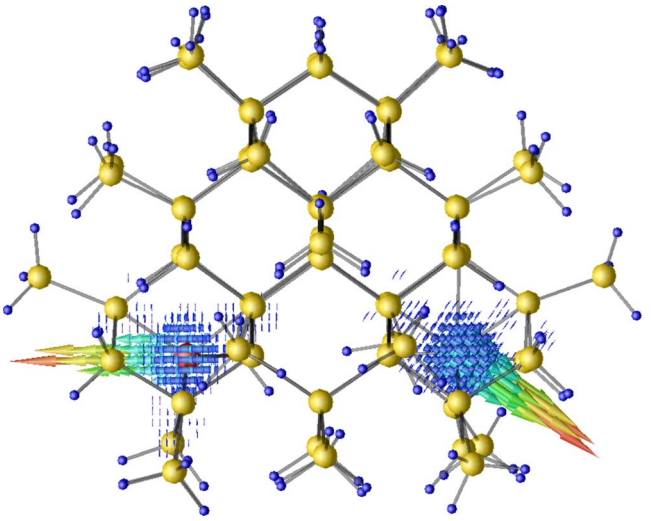

FIG. 4. (Color online) Vector-field representation of the magnetization density for the int 3.5–3.5 system. The color of the drawn vectors indicates the absolute value of the magnetization. The magnetization is well localized at the two Mn dopant sites which results in two projected magnetic moments of about 3.0 μ_B. The angle between both magnetic moments amounts to 144°.

The damped oscillating behavior of J as a function of distance d in Fig. 3 seems to indicate similarities to a RKKY mechanism. Similar oscillations were found by Stroppa *et al.*[36] for the magnetic moments induced on the group-IV atoms in Mn-doped Si and Ge host matrices. A simple curve fitting to the RKKY coupling constant[40]

$$J_{\mathrm{RKKY}} \sim \frac{1}{d^4}[2k_F d\cos(2k_F d) - \sin(2k_F d)] \tag{5}$$

with k_F as the Fermi wave vector of the surrounding electron gas is in good agreement with the observed behavior (blue line in Fig. 3). The absolute value of J in the different regions could be recovered well. The fitting procedure also provides information on the Fermi wave vector which is around $k_F=0.65$ Å^{-1}. Compared to an equivalent electron gas this corresponds to a electron concentration of about $n=\frac{k_F^3}{3\pi^2}=0.93\times10^{22}$ cm^{-2}. This value is much below the density of the electrons in "bulklike" silicon. If the characteristic distance $d_c=2.9$ Å is constrained (green line in Fig. 3; $k_F=0.78$ Å^{-1}) the fitting procedure delivers the transition from region II to III at $d=4.9$ Å and a coupling constant in region II up to 65 meV. In other words RKKY-type exchange as described by Eq. (5) is not capable to reproduce the transition distances (between the different magnetic phases) and the absolute value of the magnetic coupling constant J in region II at the same time. That means that the RKKY-type exchange mechanism can describe some characteristics of the observed magnetic coupling behavior in our system. But the details of the magnetic interaction are more complex.

This complexity is reflected in the distribution of the absolute magnetic density inside the doped Si NCs as presented in Fig. 5. The magnetic density is mainly constrained around the Mn dopant sites which results in the observed localized

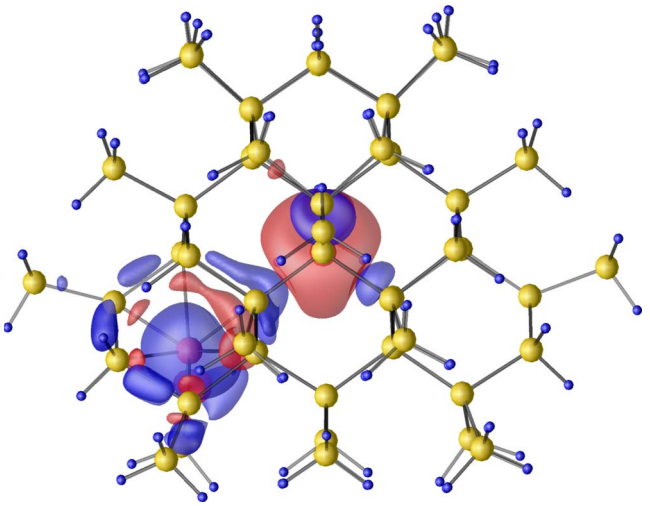

FIG. 5. (Color online) Two isosurfaces of the absolute magnetization density at the values $\pm 0.012\ e/\text{Å}^3$. The configuration of this example is the mix 1–3.5.

magnetic moments. Nevertheless, the surrounding Si atoms strongly affect the magnetic density in the NC. Substitutional dopant sites, such as the central dopant site in Fig. 5, lead to an antiferromagnetic coupling with the four nearest-neighbor Si atoms. In contrast to that, interstitial dopant sites show a more complex density distribution, e.g., some magnetic density is localized around the bonds of the surrounding Si interstitial cage. In contrast to the substitutional case the interstitial dopant site couples ferromagnetically toward the surrounding Si cage, i.e., the corresponding localized magnetic density do not change the sign. The characteristic oscillating behavior of RKKY-type coupling remains visible as the sign change in the magnetic density along a path from the Mn-dopant site toward the nearest-neighbor Si atoms.

C. Noncollinearity and magnetic moments

According to Fig. 3 and Table II noncollinear magnetism is only favored for large Mn-Mn distances $d > 4.5$ Å. Nevertheless, mostly all other Mn configurations possess local-energy minima with noncollinear arrangements of the Mn magnetic moments. The single magnetic moments $\mathbf{m}_1$ and $\mathbf{m}_2$ are thereby orientated along certain high-symmetry directions of the NC: pointing toward the central atom, a facet center, next-nearest neighbor or along crystal channels. However none of these directions is preferred throughout all noncollinear Mn-Mn configurations. The energy gain due to noncollinearity is almost negligible for small deviations from the collinear case. A comparison to collinear calculations shows that at least an angle deviation of 6° relative to the collinear direction has to be reached before a measurable energy gain can be observed. So only in the large distance case noncollinearity significantly affects the stability of the system.

Apart from the orientation dependence and, hence, the drastic variation in the total magnetic moment m_{tot} of a pairwise doped Si NC in Table II, we find that absolute values of the projected magnetic moments m_i depend on the dopant site which is occupied by the single Mn atom, i.e., substitutional or interstitial. The calculations of single-doped NCs yield values independent of the dopant site of about 3 μ_B.[14] For fourfold coordinated Mn atoms this value corresponds to the high-spin situation and, hence, Hund's rule. For Si NCs doped with Mn pairs the magnetic moments remain at this value only for int-type Mn_2 doping with values $3.0, \ldots, 3.3$ μ_B (see Table II). If substitutional sites are involved (mix- and sub-type configurations) the magnetic moments of both Mn atoms raise to $4.0, \ldots, 4.4$ μ_B (see Table II). Such a sensitivity to the local environment and the bonding configuration has been also observed for bulk Mn-containing materials.[12,41] For $Ga_{1-x}Mn_xAs$ Wu[12] reported a magnetic moment of 4.0 μ_B if the Mn atom occupies a Ga site and a value of 3.1 μ_B if Mn is placed at an interstitial site.

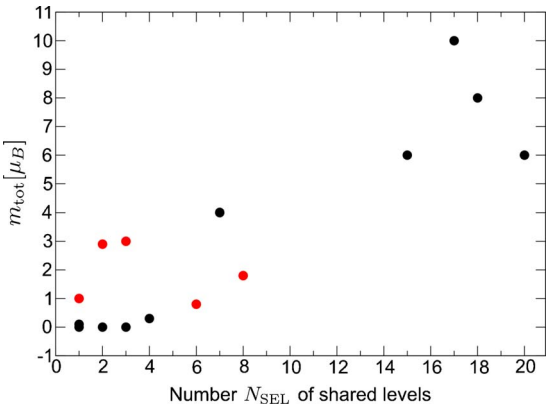

FIG. 6. (Color online) Total magnetic moment of pairwise Mn-doped Si nanocrystals with respect to the number of shared energy levels. Configurations giving noncollinear magnetism are indicated as bright red dots.

D. Shared energy levels

The magnetic exchange interaction [implicitly assumed in Eq. (4)] is mediated by the formation of shared energy levels (SEL). The wave function belonging to such a level is localized at both Mn atoms. In praxis, an energy level is called shared if the projection of its wave function on both Mn atoms lies above 10% of the total character. In a simple picture of orbital overlap one should expect a decreasing number N_{SEL} of SELs with rising Mn-Mn distance but the opposite behavior is observed. As an example the mix 3–3 configuration ($d=2.87$ Å) forms only one SEL while the int 2.5–3.5 structure ($d=4.39$ Å) shows 15 SELs, i.e., although the Mn-Mn distance rises significantly the number of SELs N_{SEL} increases. It appears that the number of SELs is actually correlated with the total magnetic moment m_{tot} of the system and not to the Mn-Mn distance. This is clearly illustrated in Fig. 6 for the Mn-Mn configurations described in Table I. For antiferromagnetic configurations with $m_{\text{tot}} \approx 0$ μ_B the number remains below $N_{\text{SEL}}=4$ (Table II region I) while ferromagnetic spin arrangements with $m_{\text{tot}} > 6$ μ_B need at least 15 SELs (Table II region II).

The unexpected relationship between N_{SEL} and m_{tot} for different Mn pair configurations needs a microscopic explanation. In the case of the antiferromagnetic mix-type dimers

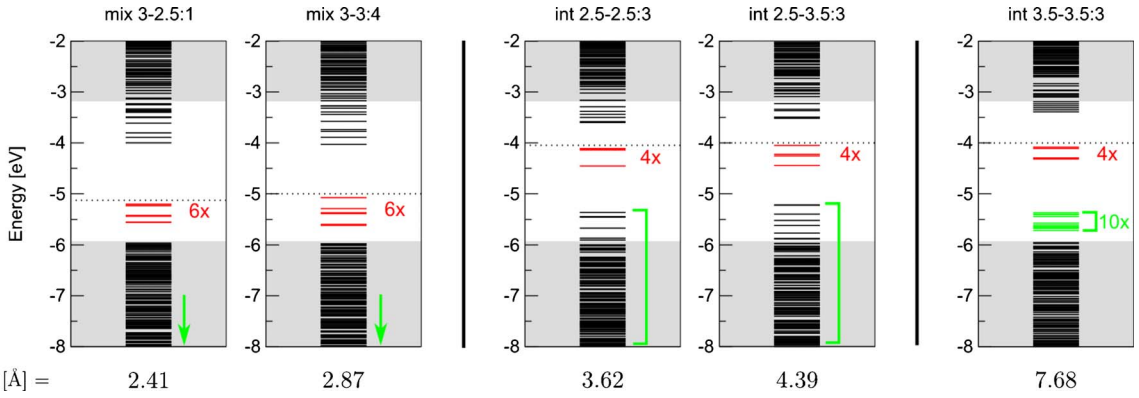

FIG. 7. (Color online) Energy-level diagrams of a pairwise doped five-shell silicon nanocrystal for selected mix and int combinations. The configuration and the Mn-Mn distance d are given. Vertical lines separate the three regions of magnetic interactions mentioned in Table II. The horizontal black lines represent the energy levels. The gray regions correspond to conduction and valence states of the undoped NC. The horizontal dotted line defines the Fermi level. The characteristic Mn-induced d-type levels near the Fermi level are indicated by red lines. The deep-lying second group of d levels is indicated by green symbols.

the energy levels of the d electrons already differ for singly doped NC systems due to the different local environments for interstitial or substitutional doping. Therefore the probability is low that d-derived states localized at one of the two Mn atoms do match in their energy and symmetry. The formation of bonding and antibonding combinations will not take place with substantial probabilities at both Mn atoms, which would characterize a SEL. The intrinsic asymmetry leads to a low number of SELs, which then mediate the antiferromagnetic coupling as delocalized states.

The situation is completely different for the combinations of Mn atoms on two interstitial or substitutional sites and not too large distances (see Table II). Those symmetric configurations, i.e., sub- and int-type dimers, show another behavior. By avoiding the mixture of substitutional and interstitial dopant sites the energy levels of the corresponding two singly doped NC systems[14] are mostly identical, thereby the absolute energy value and symmetry of the Mn-derived d states remain inside an optimal range for the creation of bonding and antibonding states. This results in the observed large number of SELs $N_{\mathrm{SEL}} \geq 15$. But due to the bigger distances the wave function of these levels are much more localized at the Mn atoms. So for these arrangements, intrinsic symmetry and Mn separation lead to many localized SELs, which mediate the ferromagnetic coupling.

E. Electronic states and magnetic properties

The calculated electronic structures due to different Mn_2 incorporations in the five-shell Si NC $Si_{83}H_{108}$ are described by energy-level diagrams in Fig. 7. The influence of the combination type (mix/int) and the changes with rising Mn-Mn distance are demonstrated. The energy scales used are absolute. They were aligned using the vacuum level as energy zero.

The most important feature of Fig. 7 is that the Mn-derived d states split off in two groups. One group of characteristic Mn $3d$ states appear in the fundamental gap directly below the Fermi energy (indicated by bright red levels). The second group consists of energetically spread d states (indicated by bright green levels). This behavior directly results in the observed strong spin polarization of about $2,\ldots,3$ eV inside singly doped Si NCs (see Ref. 14). In the simplest case the energy-level diagrams for pairwise doping can be constructed by a doubling of the diagrams obtained for the two corresponding singly doped NCs. Depending on the actual Mn pair configuration and the Mn-Mn distance the coupling between the two Mn atoms gives rise to changes in the mentioned simple doubling picture.

In the case of the mix-type doping with not too large Mn-Mn distances the first group of characteristic energy levels consists of six levels placed directly below the Fermi level as shown in the left two panels of Fig. 7. The comparison to the corresponding singly doped Si NCs (Ref. 14) shows that these six levels originate from the typically appearing four gap states of an inner substitutional dopant site (energy range: $-5,\ldots,-6$ eV) and the two gap states of the interstitial dopant site (energy range: -4.5 eV). In the pairwise doped case the wave functions belonging to these levels show an almost small d-state projection of less than 20%. Projected on the substitutional site these states exhibit a t_2 character with an additional (relative large) amount of p-orbital intermixing. This strong mixing behavior can be easily explained within a simple defect molecule model for the incorporation of a $3d$ transition-metal atom into a silicon environment with local T_d symmetry.[14,15] According to molecule model the observed orbital characteristics results of the hybridization of the symmetry-adopted t_2 states derived from the four sp^3 Si bonds and the t_2 states derived from the (substitutional) Mn $3d$ states. The strong p character (projected on the substitutional) is surprisingly not only observed at the four states corresponding to the substitutional dopant site, but on all six levels, because the influence of the Mn-Mn coupling mainly affects the energy states introduced by the interstitial Mn. Relative to the singly doped case these states are delocalized through the coupling toward the substitutional nearest-neighbor Mn atom. This results in an effective p character of the two interstitial derived states at the neighbor substitutional site and the decrease in their absolute energetic position by approximately 1 eV. For neighboring

mix configurations the six gap states are clearly allocated at the substitutional component, which results in the observed even number for the projected magnetic moments (about 4 μ_B, see Table II) in the case of mix-type combinations, as for singly Mn-doped Si NCs only odd numbers are allowed (see Ref. 14).

The missing Mn valence electrons occupy largely spread deep energy levels about 3 eV below the gap *d*-derived levels (marked green in Fig. 7). The deep levels of the corresponding isolated Mn dopants are shifted up to 2.5 eV toward lower energies. However, their wave functions show a projection onto the *d* states which are quite large (up to 50% of total character). A mapping of these levels on t_2 and *e* symmetry could not be done due to a strong intra-*d*-band mixing which leads to t_2/e ratios up to 1:1. The introduced symmetry break through the introduction of the Mn pair lifts the T_d symmetry and therefore the requirement for the t_2, *e* symmetry assignment.

The transition from antiferromagnetic mix systems toward ferromagnetic int systems (third and fourth panels of Fig. 7) is accompanied by multiple changes in the energy-level diagrams. First only four characteristic gap states appear at an energy value of about −4.0−−4.5 eV. The model of a simple doubling of the two corresponding singly doped energy diagrams holds,[14] in the sense that each isolated interstitial delivers two gap states in almost the observed energy range. The changes in this simple picture are much weaker than in the stronger interacting mix-type systems mentioned above. There is no essential energy shift with respect to the singly doped case. The shift of the levels near the Fermi energy is about or smaller than a few hundred millielectron volt. Those minor changes reflect the weaker interaction and, hence, explain the reduction in the absolute magnetic-coupling constant as shown in Table II (region II).

Due to the weaker coupling with the surrounding Si atoms (no true bonding) the *d* projection contribution is significantly larger than for mix-type systems (up to 50% of total character). Similarly to the mix case the remaining valence electrons occupy energetically spread *d* states, covering a energy region from −5 to −7 eV. Relative to the mix case they are shifted 3 eV toward higher energies. Most of the *d*-state-derived levels are SELs and, hence, are strongly localized at the Mn atoms, therefore mediating the ferromagnetic coupling.

A Mn-Mn arrangement with noncollinear magnetization yields to a different level scheme as shown in the fifth panel of Fig. 7. Since in this distance region the Mn-Mn interaction tends to vanish, both energy-level diagrams of the singly doped Si NCs are superposed without interaction of the *d* states, respectively, without any energetic splitting and shift. The vanishing mixing of states localized at different Mn atoms leads to additional ten occupied defect-related levels between Fermi energy and the top of the occupied levels of the undoped Si NC. Contrary to the combinations included in regions I and II there is no t_2-*e* intermixing in the character of the *d*-derived levels because the local T_d character is almost not lifted through some Mn-Mn interaction.

The spread and energy of the deep *d*-level group determine the type of magnetic coupling. A hugely spread group far beneath the highest occupied molecular orbital (HOMO) of the undoped NC indicates an AFM coupling, a group spread around these HOMO indicates a FM coupling and a weak spread group above HOMO will lead to the formation of noncollinear magnetism.

IV. SUMMARY

Using *ab initio* density-theory functional methods, we have calculated the energetic, electronic, and magnetic properties of Mn_2 dimers embedded in a Si nanocrystal. The magnetic moments are clearly localized at the Mn sites. The magnitude of the magnetic moments is sensitive to the site character, interstitial or substitutional. Interstitial combinations show a local magnetic moment of about 3 μ_B while substitutional doping increase the value to about 4 μ_B. The magnetic moments are more or less arranged in parallel or antiparallel configurations. Noncollinearity effects lower the total energy of the NC if the deviation angle is larger than 6°. Noncollinear configurations appear for large distances. However, the surrounding nanocrystal stabilizes those alignments even for small distances, at least in arrangements giving rise to local-energy minima.

The total magnetic moment of the pairwise doped Si NC significantly depends on the alignment of local magnetic moments. The calculations show that this alignment as well as magnetic interaction are influenced by the site character and the Mn-Mn distance. They have been characterized by the sign and the magnitude of the effective (nearest-neighbor) coupling constant $J=J(d)$. Up to $d=2.9$ Å antiferromagnetic arrangements of the two Mn spins $J<0$ are strongly favored with $J\approx-150$ meV for $d\approx2.5$ Å, mostly supported by mix-type doping. The *p*-*d*-type coupling of the substitutional Mn with the surrounding crystal enhances the sensitivity of the total energy. Therefore, small Mn-Mn distances $d<2.9$ Å lead to a wide spread of the magnetic coupling constants *J*. For distances between 2.9 and 4.5 Å ferromagnetic coupling with $J<0$ is observed accompanied by a decrease in the absolute coupling constant of about one magnitude ($J\approx+15$ meV) in comparison to the typical antiferromagnetic situation. The FM configurations are mostly built by dopant sites of equal character, i.e., sub -or int-type combination. The intrinsic symmetry and medium Mn-Mn distance of these systems result in a large number of (well-localized) shared energy levels. Above 4.5 Å the *p*-*d* coupling with the surrounding crystal prevails the Mn-Mn (*d*-*d*) coupling, therefore leading to noncollinear spin arrangements along high-symmetry orientations.

The oscillating behavior of *J* as a function of the distance *d* seems to indicate a RKKY-type exchange mechanism. However, in detail the magnetic interaction is more complex due to the influence of the silicon atoms in the NC surrounding a Mn dopant.

The electronic properties are determined by the type of the involved Mn-dopant sites and the magnetic interaction. We have demonstrated a direct relationship of the total magnetic moment of the pairwise doped NC with the formation of shared energy levels. The dopant-site type specifies the number of Mn 3*d*-derived gap states below the Fermi level. For instance, mix arrangements show six and int combina-

tions four characteristic gap levels. The position of the remaining deep *d* levels is directly related to the magnetic ordering. Antiferromagnetic mix systems show largely spread levels considerably below the HOMO level of the undoped system. A change in the magnetic coupling toward ferromagnetism (inside int combinations) leads to a shift of these levels close to the HOMO level. Due to their weak-coupling noncollinear arrangements show almost degenerate levels directly above the HOMO.

ACKNOWLEDGMENTS

The work was financially supported through the Fonds zur Förderung der Wissenschaftlichen Forschung (Austria) in the framework of SFB25, Nanostrukturen für Infrarot-Photonik (IR-ON), the Deutsche Forschungsgemeinschaft (Project No. Be1346/20-1), and the EU e-I3 ETSF project (Grant No. 211956). Grants of computer time from the Höchstleistungsrechenzentrum Stuttgart are gratefully acknowledged.

*christian.panse@uni-jena.de
†Permanent address: GWT-TUD GmbH, Abteilung Material Calculations, Annabergerstr. 240, 09125 Chemnitz, Germany.

[1] M. Bolduc, C. Awo-Affouda, A. Stollenwerk, M. B. Huang, F. G. Ramos, G. Agnello, and V. P. LaBella, Phys. Rev. B **71**, 033302 (2005).
[2] M. C. Qian, C. Y. Fong, K. Liu, W. E. Pickett, J. E. Pask, and L. H. Yang, Phys. Rev. Lett. **96**, 027211 (2006).
[3] S. C. Erwin, L. Zu, M. I. Haftel, A. L. Efros, T. A. Kennedy, and D. J. Norris, Nature (London) **436**, 91 (2005).
[4] D. J. Norris, N. Yao, F. T. Charnock, and T. A. Kennedy, Nano Lett. **1**, 3 (2001).
[5] Y. Léger, L. Besombes, L. Maingault, J. Fernández-Rossier, D. Ferrand, and H. Mariette, Phys. Status Solidi B **243**, 3912 (2006).
[6] A. Nag and D. D. Sarma, J. Phys. Chem. C **111**, 13641 (2007).
[7] J. R. Chelikowsky, E. Kaxiras, and R. M. Wentzcovitch, Phys. Status Solidi B **243**, 2133 (2006).
[8] X. Huang, A. Makmal, J. R. Chelikowsky, and L. Kronik, Phys. Rev. Lett. **94**, 236801 (2005).
[9] G. M. Dalpian and J. R. Chelikowsky, Phys. Rev. Lett. **96**, 226802 (2006).
[10] J. T. Arantes, G. M. Dalpian, and A. Fazzio, Phys. Rev. B **78**, 045402 (2008).
[11] T. O. Strandberg, C. M. Canali, and A. H. MacDonald, Phys. Rev. B **81**, 054401 (2010).
[12] R. Wu, Phys. Rev. Lett. **94**, 207201 (2005).
[13] L. Ma, J. Zhao, J. Wang, B. Wang, and G. Wang, Phys. Rev. B **75**, 045312 (2007).
[14] R. Leitsmann, C. Panse, F. Küwen, and F. Bechstedt, Phys. Rev. B **80**, 104412 (2009).
[15] R. Leitsmann, F. Küwen, C. Rödl, C. Panse, and F. Bechstedt, J. Chem. Theory Comput. **6**, 353 (2010).
[16] M. Jamet *et al.*, Nature Mater. **5**, 653 (2006).
[17] H. Wu, M. Hortamani, P. Kratzer, and M. Scheffler, Phys. Rev. Lett. **92**, 237202 (2004).
[18] H. Wu, P. Kratzer, and M. Scheffler, Phys. Rev. Lett. **98**, 117202 (2007).
[19] F. Küwen, R. Leitsmann, and F. Bechstedt, Phys. Rev. B **80**, 045203 (2009).
[20] Y. D. Park, A. T. Hanbicki, S. C. Erwin, C. S. Hellberg, J. M. Sullivan, J. E. Mattson, T. F. Ambrose, A. Wilson, G. Spanos, and B. T. Jonker, Science **295**, 651 (2002).
[21] Y.-J. Zhao, T. Shishidou, and A. J. Freeman, Phys. Rev. Lett. **90**, 047204 (2003).
[22] M. C. Payne, M. P. Teter, D. C. Allan, T. A. Arias, and J. D. Joannopoulos, Rev. Mod. Phys. **64**, 1045 (1992).
[23] L. E. Ramos, J. Furthmüller, and F. Bechstedt, Phys. Rev. B **72**, 045351 (2005).
[24] L. E. Ramos, H. Weissker, J. Furthmüller, and F. Bechstedt, Phys. Status Solidi B **242**, 3053 (2005).
[25] G. Kresse and J. Furthmüller, Comput. Mater. Sci. **6**, 15 (1996).
[26] D. Hobbs, G. Kresse, and J. Hafner, Phys. Rev. B **62**, 11556 (2000).
[27] Y. Xie and J. A. Blackman, Phys. Rev. B **73**, 214436 (2006).
[28] A. Filipponi, M. Borowski, and F. Natali, Phys. Rev. B **60**, 6 (1999).
[29] A. Stroppa and M. Peressi, Phys. Status Solidi A **204**, 44 (2007).
[30] C. Zeng, S. C. Erwin, L. C. Feldman, A. P. Li, R. Jin, Y. Song, J. R. Thompson, and H. H. Weitering, Appl. Phys. Lett. **83**, 5002 (2003).
[31] G. Kresse and D. Joubert, Phys. Rev. B **59**, 1758 (1999).
[32] S. L. Dudarev, G. A. Botton, S. Y. Savrasov, C. J. Humphreys, and A. P. Sutton, Phys. Rev. B **57**, 1505 (1998).
[33] J. Okabayashi, A. Kimura, T. Mizokawa, A. Fujimori, T. Hayashi, and M. Tanaka, Phys. Rev. B **59**, R2486 (1999).
[34] U. von Barth and L. Hedin, J. Phys. C **5**, 1629 (1972).
[35] I. Appelbaum, B. Huang, and D. J. Monsma, Nature (London) **447**, 295 (2007).
[36] A. Stroppa, S. Picozzi, A. Continenza, and A. J. Freeman, Phys. Rev. B **68**, 155203 (2003).
[37] F. Bernardini, S. Picozzi, and A. Continenza, Appl. Phys. Lett. **84**, 2289 (2004).
[38] J. Mejía-López, A. H. Romero, M. E. Garcia, and J. L. Morán-López, Phys. Rev. B **74**, 140405 (2006).
[39] P. Wahl, P. Simon, L. Diekhöner, V. S. Stepanyuk, P. Bruno, M. A. Schneider, and K. Kern, Phys. Rev. Lett. **98**, 056601 (2007).
[40] M. A. Ruderman and C. Kittel, Phys. Rev. **96**, 99 (1954).
[41] A. Stroppa, X. Duan, and M. Peressi, Mater. Sci. Eng., B **126**, 217 (2006).